Minimizing actuator-induced errors in active space telescope mirrors

Citation: Smith, Matthew W., and David W. Miller. "Minimizing actuator-induced errors in active space telescope mirrors." Space Telescopes and Instrumentation 2010: Optical, Infrared, and Millimeter Wave. Ed. Jacobus M. Oschmann et al. San Diego, California, USA: SPIE, 2010. 773122-14. © 2010 SPIE

As Published: http://dx.doi.org/10.1117/12.855947

Publisher: SPIE

Persistent URL: http://hdl.handle.net/1721.1/61645

Version: Final published version: final published article, as it appeared in a journal, conference proceedings, or other formally published context

Minimizing actuator-induced errors in active space telescope mirrors

Matthew W. Smith and David W. Miller

Massachusetts Institute of Technology, 77 Massachusetts Ave, Cambridge, MA 02139

ABSTRACT

The trend in future space telescopes points toward increased primary mirror diameter, which improves resolution and sensitivity. However, given the constraints on mass and volume deliverable to orbit by current launch vehicles, creative design solutions are needed to enable increased mirror size while keeping mass and volume within acceptable limits. Lightweight, segmented, rib-stiffened, actively controlled primary mirrors have emerged as a potential solution. Embedded surface-parallel actuators can be used to change the mirror prescription on-orbit, lowering mirror mass overall by enabling lighter substrate materials such as silicon carbide (SiC) and relaxing manufacturing constraints. However, the discrete nature of the actuators causes high spatial frequency residual errors when commanding low-order prescription changes. A parameterized finite element model is used to simulate actuator-induced residual error and investigate design solutions that mitigate this error source. Judicious specification of mirror substrate geometry and actuator length is shown to reduce actuator-induced residual while keeping areal density constant. Specifically, a sinusoidally-varying rib shaping function is found to increase actuator influence functions and decrease residual. Likewise, longer actuators are found to offer reduced residual. Other options for geometric shaping are discussed, such as rib-to-facesheet blending and the use of two dimensional patch actuators.

Keywords: Active mirrors, actuator-induced residual error, finite element modeling, surface-parallel actuators, cryogenic SiC mirrors.

1. INTRODUCTION

Space-based optical telescopes, like their ground-based counterparts, are typically designed with an emphasis on maximizing aperture diameter. Larger apertures allow increase telescope resolution and sensitivity, two critical figures of merit for high quality imaging. However unlike ground systems, space telescopes are severely constrained by launch vehicle mass and volume limits. This necessitates creative design solutions for increasing aperture area with minimal corresponding mass and volume growth. Current approaches are the use of a segmented primary mirror that launches in a compact stowed configuration and unfolds on orbit—addressing the volume constraint—and low areal density mirror design—addressing the mass constraint. The challenge then becomes preserving optical performance in the presence of these design changes. Thus designing compact, lightweight, yet optically precise primary mirrors for space telescopes presents a significant challenge. This work offers solutions, particularly for the mass-constrained (i.e. low areal density) case.

Over the past few decades, reaction bonded silicon carbide (SiC) has emerged as a promising material for space telescope mirrors.[1] It has a relatively low coefficient of thermal expansion (CTE), high thermal conductivity, a high elastic modulus, and relatively low density.[2] When an SiC substrate is augmented by embedded surface-parallel electrostrictive actuators, the result is a highly integrated active mirror system that can undergo changes in optical prescription—e.g. changes in radius of curvature (RoC)—without the need for a bulky reaction structure.[3] These actuators allow for on-orbit correction of figure errors due to CTE effects in a changing thermal environment, or due to RoC mismatch from the manufacturing process.

Further author information: (Send correspondence to M. Smith)
M. Smith: E-mail: m_smith@mit.edu, Telephone: 1 626 665 3201
D. Miller: E-mail: millerd@mit.edu, Telephone: 1 617 253 3288

Space Telescopes and Instrumentation 2010: Optical, Infrared, and Millimeter Wave,
edited by Jacobus M. Oschmann Jr., Mark C. Clampin, Howard A. MacEwen, Proc. of SPIE
Vol. 7731, 773122 · © 2010 SPIE · CCC code: 0277-786X/10/$18 · doi: 10.1117/12.855947

1.1 Actuator-induced residual error

While highly integrated active SiC mirrors offer tremendous promise in terms of low areal density and manufacturing cost, complications arise as a result of actuator behavior. Specifically, the discrete placement and local influence of the actuators makes it difficult to command perfectly smooth low-order changes such as RoC adjustments. This is depicted in Figure 1.

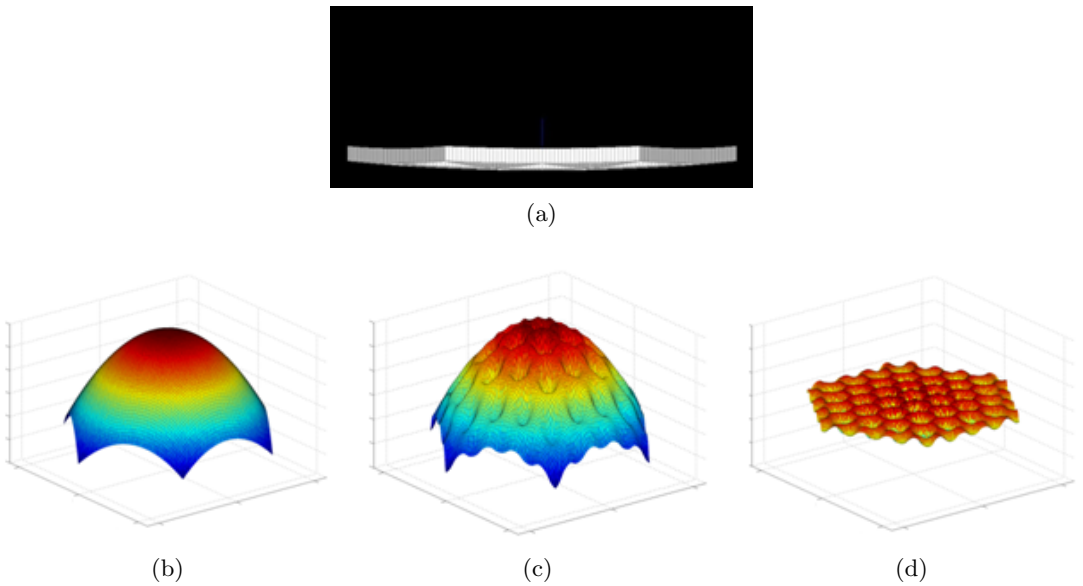

(a) (b) (c) (d)

Figure 1. (a) Edge-on view of an un-deformed mirror with upward concavity due to its radius of curvature, (b) desired surface change for positive ΔRoC, (c) actual surface change for positive ΔRoC with discrete actuators, and (d) actuator-induced residual error (difference of b and c).

.

Figure 1(a) shows a rib stiffened active mirror segment from an edge-on view. The reflecting surface is on the top of the mirror in this view, with slight upward concavity due to a parabolic optical figure. A phasing maneuver may require an increase in RoC, which is equivalent to seeking the mirror surface displacements shown in Figure 1(b): for an increase in RoC, the mirror is made "flatter" by commanding the edges to deflect downward. Because of the discrete locations and localized influence of the actuators, however, the actual displacement is the shape shown in Figure 1(c). Instead of being smooth, the actual displacements more resemble the surface of a golf ball, with the actuators introducing an unwanted high spatial frequency variation on top of the desired low order shape. The difference between the optically perfect desired surface change and the actual surface change is termed actuator-induced residual error, or actuator "quilting". This residual error acts as an optical aberration, degrading the image quality.

1.2 Objective

Thus the challenge is to preserve the ability to command low-order shape changes while simultaneously reducing high spatial frequency residual error caused by the actuators. If actuator-induced residual is too large, the operational benefits from having an adjustable mirror prescription are quickly negated. Furthermore, any residual mitigation should ideally be accomplished without adding to the mass or complexity of the mirror system. Recent work[4,5] points to creative design of mirror geometry via finite element modeling as one possible way to decrease actuator-induced residual. Therefore the objective of this work is the to reduce actuator-induced high spatial frequency residual error by manipulating mirror geometry using a parametric finite element model, while keeping areal density and number of actuators constant.

2. PRIOR WORK

The effort described here draws on prior research using the Modular Optical Space Telescope (MOST) finite element model developed at the MIT Space Systems Laboratory (SSL). A high fidelity, parameterized representation of lightweight space telescope primary mirrors, MOST allows for the rapid generation and evaluation of rib-stiffened, actively controlled designs across the trade space. Cohan[6,7] uses the MOST model along with vibroacoustic analysis to determine optimal mirror designs for launch survival and on-orbit performance. Likewise, Gray[4,8] considers high-spatial frequency errors due to actuator and manufacturing effects. After determining the parameters with the largest influence on overall residual error, optimizations are carried out to derive a set of optimal design relationships that minimize uncorrectable high spatial frequency error while satisfying manufacturing constraints. Much of the modeling infrastructure used in the present work has heritage from the above MOST investigations.

Finite element (FE) modeling has been previously employed by a number of authors to analyze mirror design. Nied and Rudmann[9] use FE models to characterize thermal distortions in the Hubble Space Telescope (HST) primary mirror. Shepherd et al.[10] construct an FE representation of a actively controlled membrane mirror, and use the model to validate a novel modal transformation method for describing mirror displacements. Finally, Jordan and Miller[11] use an FE model to demonstrate the feasibility of mirror figure control using embedded strain gauges and temperature sensors.

These simulation-based results complement a large body of prior work on rib-stiffened hardware pathfinders. The Subscale Beryllium Mirror Demonstrator (SBMD) demonstrated enabling technologies for lightweight cryogenic mirrors as a precursor to the James Webb Space Telescope (JWST). With a diameter of approximately 0.5 m and an adjustable RoC, the SBMD showed, among other requirements, a surface figure roughness of less than $\lambda/4$ p-v at $\lambda = 633$ nm under cryogenic vacuum conditions.[12] Experience from SBMD was applied to the Advanced Mirror System Demonstrator (AMSD), a 1.4 m diameter rib-stiffened beryllium hexagonal mirror segment with four degrees of freedom (piston, tip/tilt, RoC). Cryogenic performance of this mirror also met requirements and results were used to guide JWST segment design.[13] Finally, the Primary Mirror Segment Assembly (PMSA) demonstrated TRL-6 for the JWST primary mirror by verifying segment requirements in a space-equivalent thermal and vacuum environment.[14,15]

Of particular relevance to the present study is the work of Budinoff and Michels[5] and Park et al.,[16] both of which consider optimization over geometric design parameters to reduce residual figure error. Budinoff and Michels demonstrate a significant reduction in actuator-induced residual for the Spherical Primary Optical Telescope (SPOT) segment. The authors create a finite element model of the cast Pyrex mirror substrate and parameterize the back surface shape using a series of basis functions that define the substrate thickness. By coupling the parameterized model with an optimization routines, they determine the mirror substrate geometry that minimizes residual caused by the single surface-normal actuator used for RoC changes. Park et al. likewise reduce mirror surface errors via finite element modeling and geometry optimization. In this case, however, the authors attempt to mitigate errors due to gravity sag and manufacturing print-through rather than actuator effects. Neither Budinoff and Michels nor Park et al. consider geometry variation for active rib-stiffened mirrors, which is the subject of this work.

3. MIRROR MODELING APPROACH

Figure 2 below shows the approach to mirror modeling. A parametric finite element mirror model lies at the center of the process. The user passes to the model a single input file that contains parameters defining high-level properties of the mirror (e.g. areal density, number of actuators, substrate geometry, segment diameter, etc). These parameters are passed to model that automatically constructs a finite element representation of the desired mirror in MSC.Nastran. This work assumes the use of reaction bonded SiC as the mirror substrate, given the benefits identified in Section 1. The FE solver is used to generate a number of user-selectable figures of merit; residual error is used in this work. The parametric and automated nature of the FE model allows for rapid design iteration, either by varying parameters of interest to explore the trade space or by using an optimization routine to minimize a user-defined cost function.

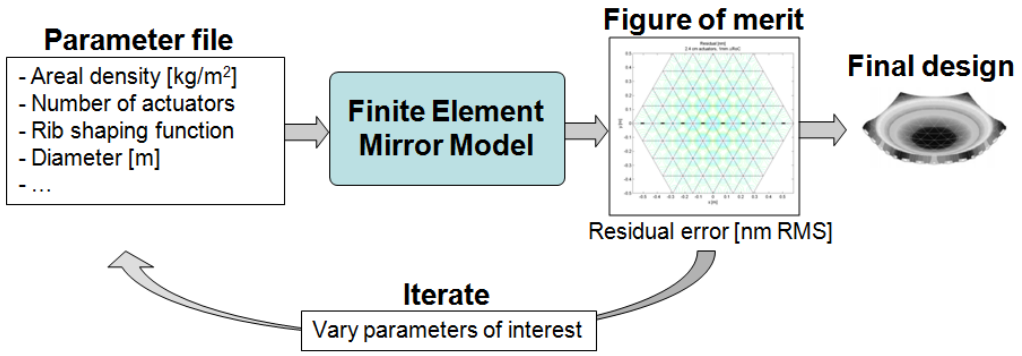

Figure 2. Design process supported by the MOST finite element mirror model.

3.1 Baseline mirror

Table 1 shows the parameters of the baseline mirror used in this thesis. It consists of a 1.0 m diameter (flat-flat) substrate with 156 embedded actuators. The areal density of the SiC substrate alone is 8 kg/m^2. The embedded actuators add 2 kg/m^2, miscellaneous cabling and electronics add 1 kg/m^2, and the three kinematic bipod position actuators add 1 kg/m^2, approximately.[1] The total areal density of the baseline mirror segment is therefore approximately 12 kg/m^2.

Table 1. Baseline mirror parameters.

Parameter	Baseline value
Diameter (flat-flat)	1.0 m
Areal density (SiC substrate only)	8 kg/m^2
Radius of curvature	6 m
Rib cell length	14.4 cm
Rib height	25.4 mm
Rib thickness	1 mm
Facesheet thickness	1.8 mm
Number of actuators	156
Actuator length	7.2 cm
Actuator length (fraction of rib cell)	0.5

3.2 Finite element implementation

Figure 3(a) shows the finite element implementation of the baseline mirror. The view is of the rib-stiffened back structure, with the reflecting surface pointing into the page. Surface-parallel electrostrictive actuators are bonded to the center of the rib cells along the edge furthest from the facesheet; they are highlighted in Figure 3(a) by dark lines.

The mirror substrate is modeled as a collection of Nastran plate elements. Details of the finite element construction for a rib section are shown in Figure 3(b). The facesheet is constructed from triangular CTRIA3 elements in order to match the triangular symmetry of the facesheet regions between ribs. The ribs are modeled using quadrilateral CQUADR elements that intersect the facesheet elements at right angles. The actuators are modeled as one dimensional CBAR elements anchored to the edge nodes of the rib quadrilateral elements. Piezoelectric strains are not directly supported by MSC.Nastran, therefore a thermal analogy is used wherein the application of temperature commands and subsequent strains due to CTE effects mimic the behavior of

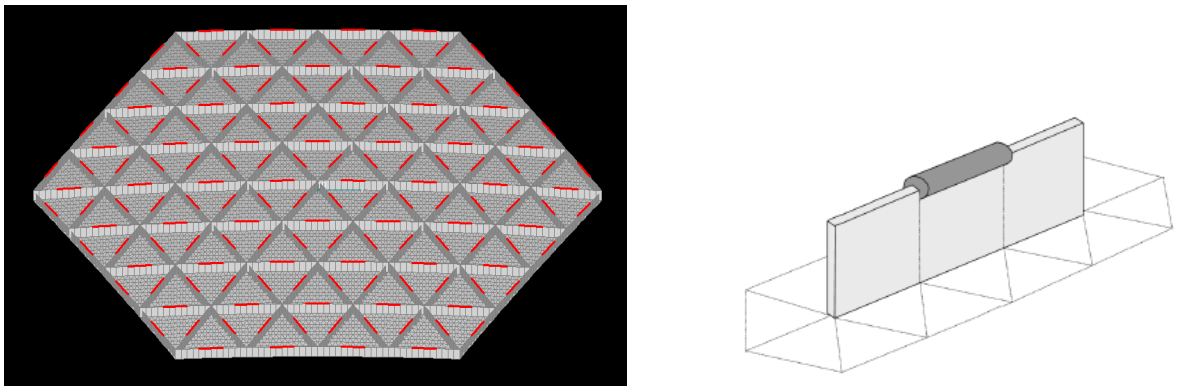

(a) (b)

Figure 3. (a) Finite element mirror model for the baseline mirror and (b) rib, facesheet, and actuator detail[4] showing triangular, quadrilateral, and rod elements.

electrostrictive material. Ĉoté et al.[17] describe the modeling process in detail and experimentally validate the thermal/piezo strain equivalence relationships.

The MOST mirror model has been tested for proper convergence with increasing mesh density. Furthermore, the model has been validated by comparing key figures of merit against empirical data. Specifically, the fundamental frequency of the mirror model matched that of a laboratory article within approximately 2% and the residual wavefront error for a given RoC command matched within approximately 7%.[7]

3.3 Command and residual calculation

This work assumes that low-order changes to the mirror shape are commanded in order to correct quasi-static disturbances such as thermal distortion, therefore the control bandwidth is relatively low. A radius of curvature change (ΔRoC) of 1 mm is chosen as a representative maneuver from which the actuator-induced residual is calculated. The embedded actuators can be used to command other low-order shape changes, however ΔRoC is used as a baseline in this case.

If the mirror surface shape is parameterized by a desired set of node displacements $\bar{z}$ in the optical axis direction z, then the actuator commands $\bar{u}$ for achieving those displacements are given by the solution to,

$$H\bar{u} + \bar{z} = \bar{0} \tag{1}$$

Here H is the matrix of influence functions calculated by displacing each actuator individually using a known input and measuring the resulting mirror displacement at each surface node. Figure 4(a) shows an influence function for one actuator. Solving (1) for the commands $\bar{u}_{+1\text{ mm}}$ needed to actuate 1 mm ΔRoC (i.e. the node displacements $\bar{z}_{+1\text{ mm}}$) gives,

$$\bar{u}_{+1\text{ mm}} = -\left(H^T H\right)^{-1} H^T \bar{z}_{+1\text{ mm}} \tag{2}$$

where it is necessary to use the Moore-Penrose pseudoinverse $\left(A^T A\right)^{-1} A^T$ because H is non-square; the number of surface nodes is typically much greater than the number of embedded actuators.

Due to the discrete nature of the embedded piezoelectric actuators, the actual mirror displacements resulting from the application of the command set (2) and the desired mirror displacements $\bar{z}_{+1\text{ mm}}$ will not be equivalent (see Figure 4). The difference between the desired and actual surface displacements in the presence of a 1 mm ΔRoC command is the actuator-induced residual error, shown in Figure 4(b). The following sections address changes in actuator and substrate geometry that mitigate actuator quilting in rib-stiffened mirrors.

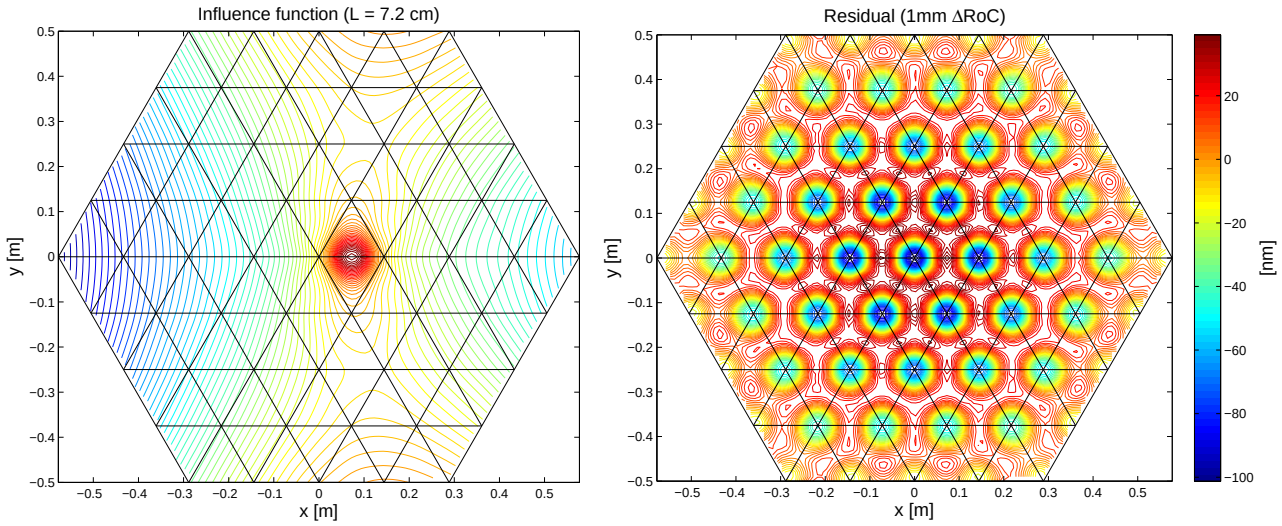

(a) (b)

Figure 4. (a) Influence function, i.e. the mirror displacement due to a single 7.2 cm long actuator, and (b) residual error [nm] for the baseline mirror after a 1 mm ΔRoC

4. ACTUATOR LENGTH VARIATION

When exploring variations in actuator geometry, changing actuator length is a natural place to begin. Gray[4] showed that in rib-stiffened mirrors of the type discussed here, increasing actuator length generally reduces actuator-induced residual error. This section presents additional results using the MOST mirror model and interpret findings by considering actuator influence functions.

Actuator length is an adjustable parameter in the finite element mirror model used for this analysis. A range of actuator lengths from 2.4 cm to 12.0 cm was modeled, as given in Table 2. Note that each actuator is modeled

Table 2. Modeled range of actuator lengths in units of physical distance, number of rib elements, and fraction of rib cell. Note that for the baseline mirror, the rib cell length is 14.4 cm.

Physical length [cm]	No. of rib elements [#]	Rib cell fraction [-]
2.4	2	0.17
4.8	4	0.33
7.2	6	0.50
9.6	8	0.67
12.0	10	0.83

as a single bar element that spans an integer number of quadrilateral elements in the mirror rib. The sub-section of a rib that lies between two rib intersections is termed here a *rib cell*. Therefore each rib cell houses a single actuator. In addition to defining actuator length by units of physical distance, it is possible to define the actuator according to the fraction of its rib cell that it occupies. The arrangement of an actuator within a rib cell is shown for three different lengths in Figure 5.

Given the above range of actuator lengths, the actuator-induced residual error was calculated in each case for $\Delta\text{RoC} = 1$ mm. The results are given in Figure 6. Increasing the actuator length from the baseline value of 7.2 cm to 12.0 cm decreases the actuator quilting from 25.4 nm RMS to 7.2 nm RMS—a 72% reduction. Likewise, moving from 2.4 cm actuators (quilting = 43.3 nm RMS) to 12.0 cm actuators results in a 83% reduction. The reduced residual for longer actuators can be seen directly in Figure 6(b), which shows slices through the $y = 0$

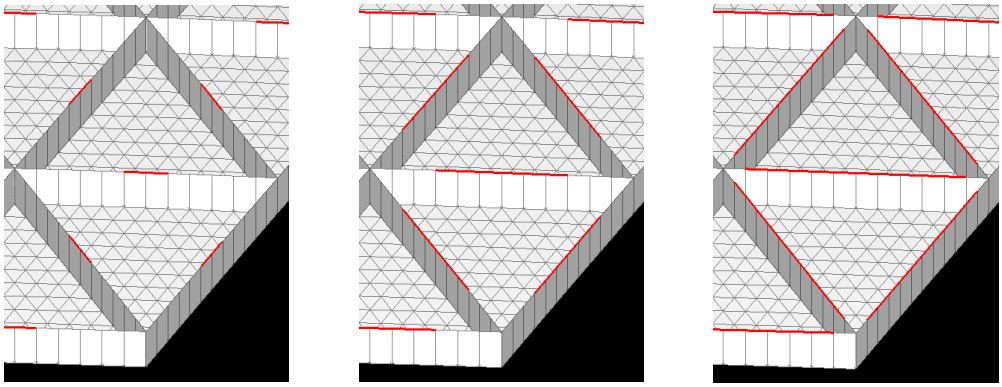

(a) (b) (c)

Figure 5. Varying actuator length l in the MOST model: (a) $l = 2.4$ cm, (b) $l = 7.2$ cm (the baseline actuator length), and (c) $l = 12.0$ cm

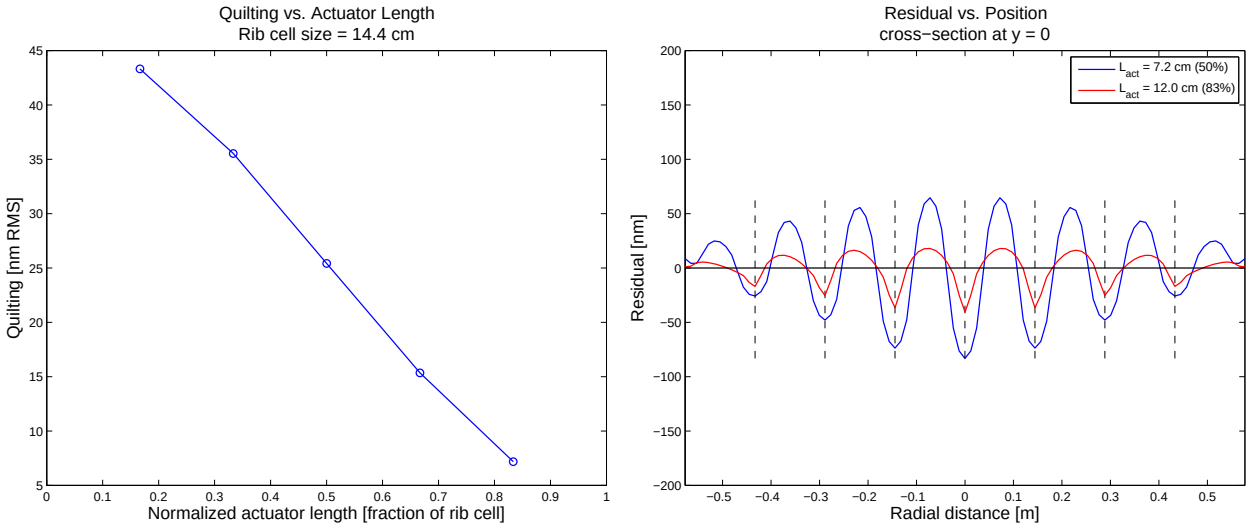

(a) (b)

Figure 6. (a) Actuator-induced residual error [nm RMS] as a function of actuator length and (b) slice of the residual contour for $l = 7.2$ cm and $l = 12.0$ cm at $y = 0$ showing decreased residual for the longer actuator case. In (b) the vertical dashed lines represent the location of rib intersections.

line of the residual contour (e.g. Figure 4). Comparing the baseline mirror ($l = 7.2$ cm) to the best performing mirror ($l = 12.0$ cm), there is a clear reduction in the magnitude residual error at all points within the mirror surface.

Looking at the changing influence function of a given actuator when altering its length can offer additional insights into the reduction in actuator quilting. Two influence functions for the same actuator with different lengths are shown in Figure 7. Figure 7(a) shows the influence function for $l = 7.2$ cm and Figure 7(b) shows the influence function for $l = 12.0$ cm. Comparing those two figures, the longer actuator yields a larger region of influence, as indicated by the wider contour spacing. Taking horizontal and vertical slices along the dashed lines indicated produces Figure 7(c) and (d), respectively. Considering Figure 7(c), a slice of the contour at $y = 0$ clearly reveals that the longer actuator has the effect of broadening the region of influence along the rib in which the actuator is situated. Likewise, Figure 7(d) shows a similar, albeit less pronounced, effect in the direction perpendicular to the rib (i.e. into the center of the triangular facesheet region on either side of the

rib). By increasing the influence function in two dimensions, lengthening the actuator provides better actuation coverage over the mirror surface. The result is an ability to command low-order prescription changes with reduced actuator-induced quilting.

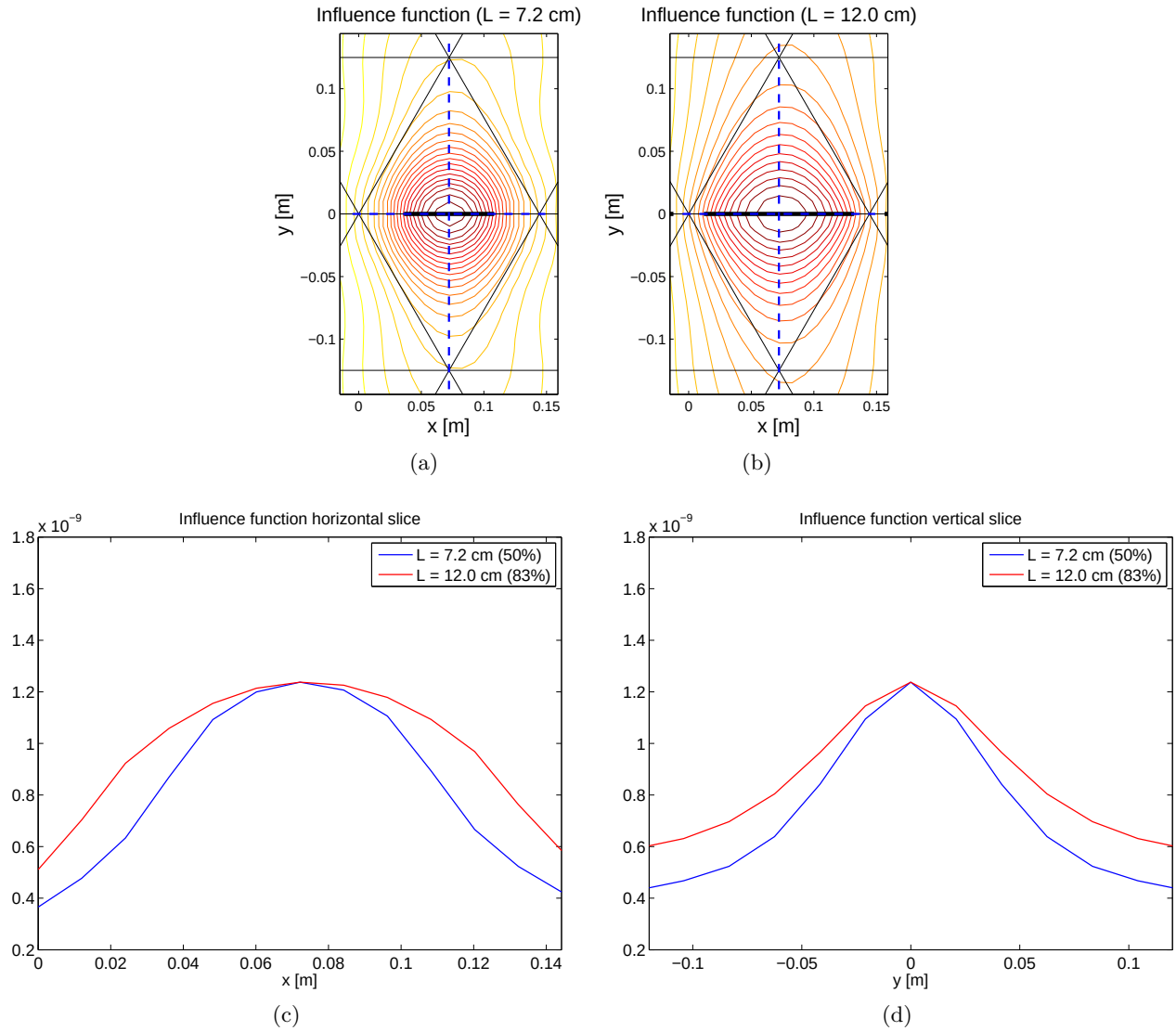

Figure 7. (a) Influence functions for actuator length $l = 7.2$ cm and (b) $l = 12.0$ cm; the view is zoomed in and the thick horizontal bar represents the actuator location. (c) Comparing horizontal slices of the two influence functions and (d) comparing vertical slices of the two influence functions.

5. SUBSTRATE GEOMETRY VARIATION

The above section considered the effects of lengthening surface-parallel actuators in rib stiffened mirrors. Benefits in terms of reduced actuator quilting are seen in the case of actuators that occupy a larger portion of the rib cell in which they reside. Lengthening actuators, however, may not always be feasible due to manufacturing constraints. This section presents altering substrate geometry as a means of reducing actuator-induced residual error while keeping actuator length constant.

As mentioned above, Budinoff and Michels[5] reduced actuator-induced residual by altering the substrate geometry to spread actuator loads more evenly. A similar approach for the case of rib-stiffened mirrors is presented here. The "basis function" describing the substrate geometry in this case is a sinusoidal variation in rib height with a period equal to a single rib cell (see Figure 8). The rib shape is parameterized by the amplitude of the variation a, where the modeled values are $a = \{0, 2.5, 5, 7.5, 10, 12.5, 15, 17.5, 20\}$ mm. In each case the mass of the substrate stays constant, therefore so does the mirror areal density.

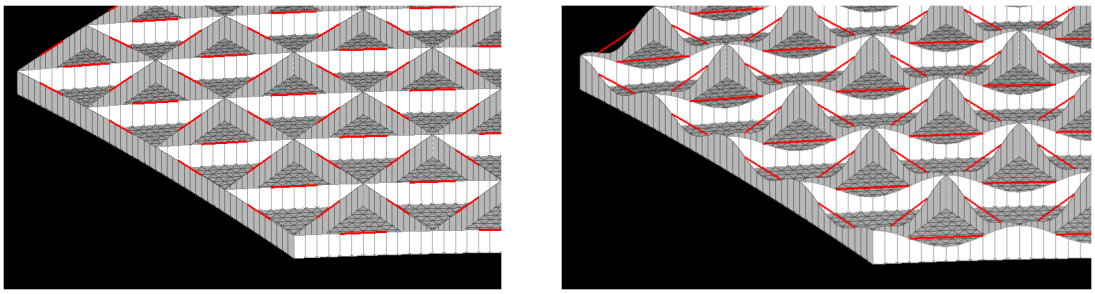

(a) (b)

Figure 8. (a) Rib shape with $a = 0$ mm (i.e. constant rib height) and (b) rib shape with $a = 10$ mm (sinusoidal variation in rib height).

As before, the actuator-induced residual was calculated for each a value given a baseline maneuver of 1 mm ΔRoC. The results are shown in Figure 9. The shaping amplitude value that minimizes the actuator-induced residual is $a = 12.5$ mm. As a increases and material is moved from the center of the ribs toward the rib intersections, each actuator is effectively lengthened, which decreases quilting for the reasons discussed in Section 4. However if too much material is removed, the ribs lose their stiffening qualities, which is detrimental to actuator-induced residual. For this mirror, $a = 12.5$ mm balances these two effects. Increasing the shaping amplitude from $a = 0$ mm (25.4 nm RMS residual) to $a = 12.5$ mm (18.6 nm RMS residual) decreases actuator-induced quilting by 27%.

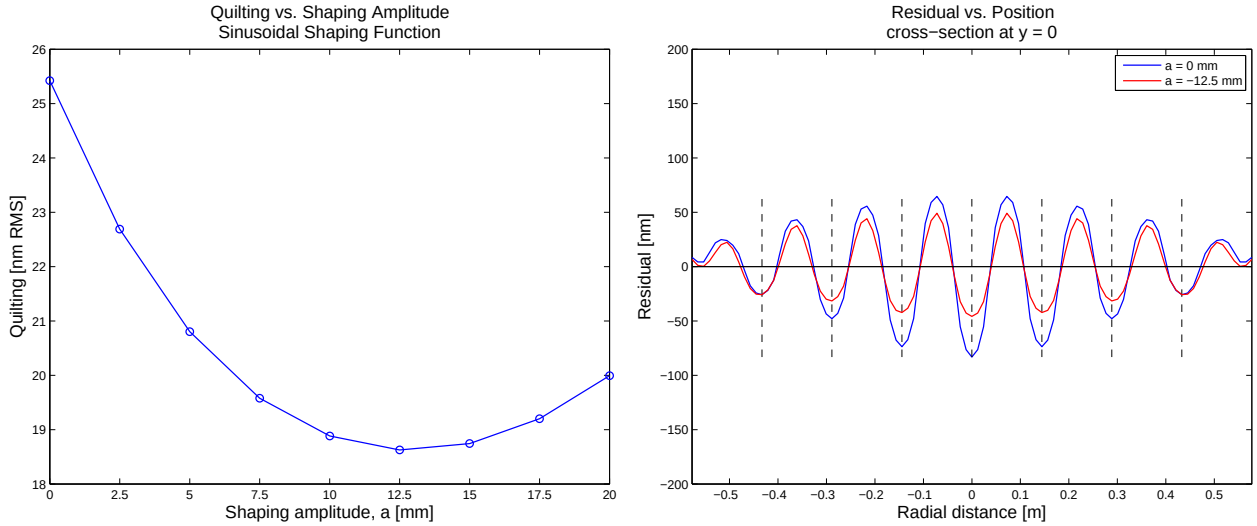

(a) (b)

Figure 9. (a) Actuator-induced residual error [nm RMS] as a function of sinusoidal rib shaping amplitude (b) slice of the residual contour for $a = 0$ mm and $a = -12.5$ mm at $y = 0$. In (b) the vertical dashed lines represent the location of rib intersections.

As before, additional insights can be gained by examining the influence functions of the baseline and optimized mirrors. These are shown in Figure 10. Comparing the contour plots of the influence functions—Figures 10(a) and (b)—the difference between the baseline and optimized case is not as pronounced as when varying actuator length. However, the larger contour spacing in Figure 10(b) indicates a broader influence function for the $a = 12.5$ case. This is reflected in the horizontal and vertical slices through the contours, shown in Figures 10(c) and (d), respectively. While the horizontal influence function expansion along ribs is smaller than the case of lengthening actuators, it nonetheless exists when shaping is added. The same applies for vertical spread of the influence function into adjacent facesheet regions. Thus while the results are less drastic than actuator lengthening, sinusoidal rib shaping does have benefits in terms of influence function spread, which in turn reduces actuator-induced residual.

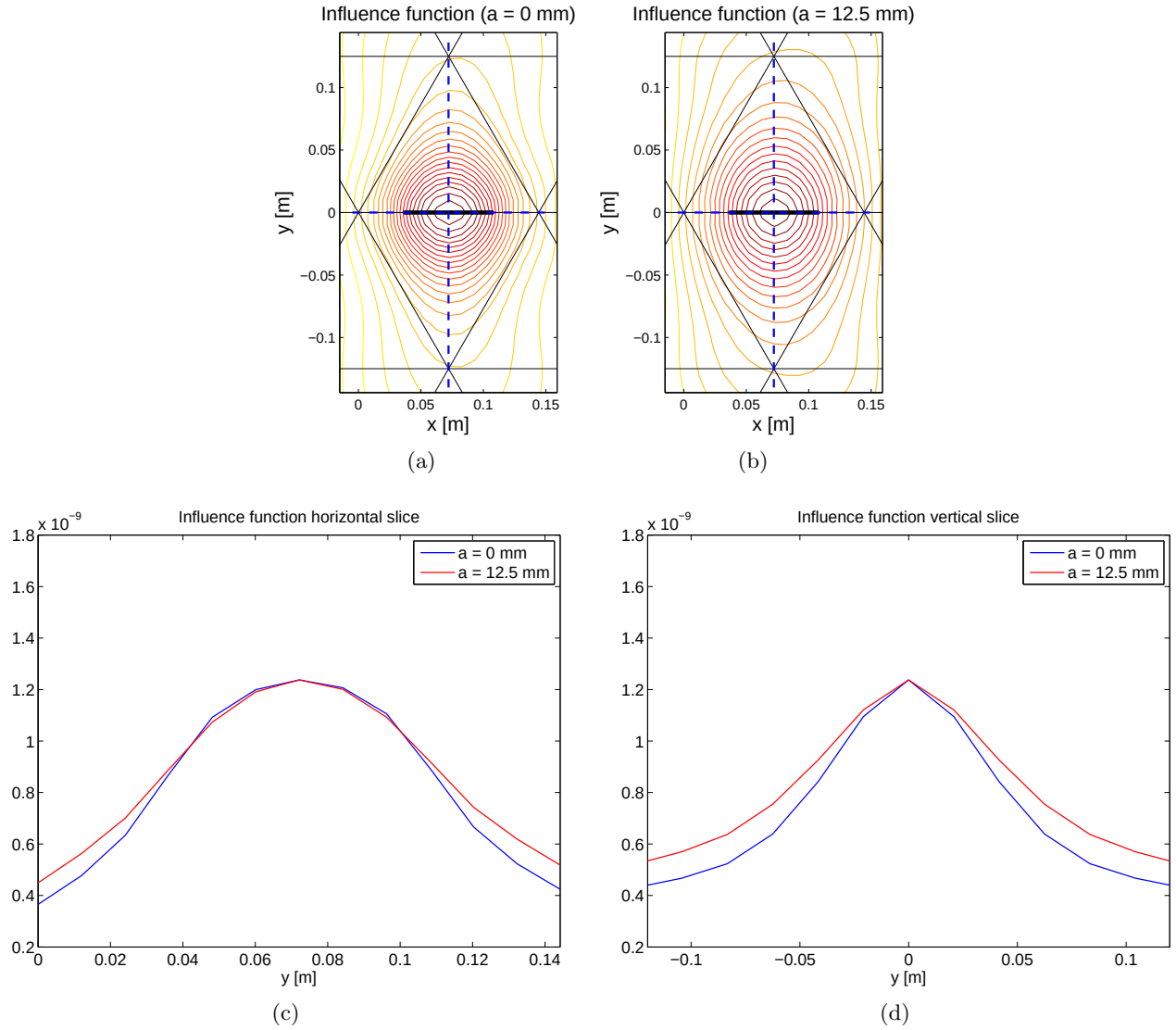

Figure 10. (a) Influence functions for constant rib height $a = 0$ mm and (b) optimal shaping amplitude $a = 12.5$ mm. (c) Comparing horizontal slices of the two influence functions and (d) comparing vertical slices of the two influence functions.

6. CONCLUSIONS AND FUTURE WORK

It has been demonstrated that changes to mirror substrate and actuator geometry can reduce actuator-induced residual errors in rib-stiffened active primary mirrors. Increasing the length of embedded surface-parallel actuator from 50% to 83% of a rib cell decreases residual errors for 1 mm ΔRoC by 73% for the mirror studied. This is due to a broadening of the localized actuator influence functions, providing better coverage over the mirror surface for low-order prescription changes.

Likewise, initial variations in substrate geometry show promise for reducing actuator-induced residual. A sinusoidally-varying height pattern was added to the ribs. Compared to the baseline (constant rib height), actuator quilting was reduced 27% by using an aplitude variation 12.5 mm. While incorporating geometric variations of this type in rib-stiffened SiC substrates may pose manufacturing difficulties, it nonetheless could reduce actuator-induced residual while keeping areal density and number of actuators constant.

6.1 Patch actuators

Surface-parallel actuators of the type discussed to this point take advantage of the d_{33} effect of electrostrictive materials—i.e. that voltage across a given axis will produce a strain in that same axis. Others have investigated the use of the d_{31} property of electrostrictive actuators, whereby the material undergoes strain in a plane normal to the voltage application. In such arrangements, two dimensional "patch" actuators bonded to reflective surfaces are used to locally alter mirror curvature. Dürr et al.[18] and Shepherd et al.[10] provide two examples.

Electrostrictive patch actuators would be a natural addition to rib-stiffened mirrors. Surface-parallel rod type actuators create influence functions that are situated on the ribs, which leaves pockets of deflection in the inter-rib locations. Placing a patch actuator in each triangular region of the face sheet between ribs would provide another set of influence functions that could aid in the actuation of smoother shape changes. The location of a single patch actuator on the facesheet opposite the reflecting surface is shown in Figure 11. In an actual implementation, the entire back side of the mirror facesheet would be covered with patch actuators to augment the cylindrical actuators distributed among the ribs.

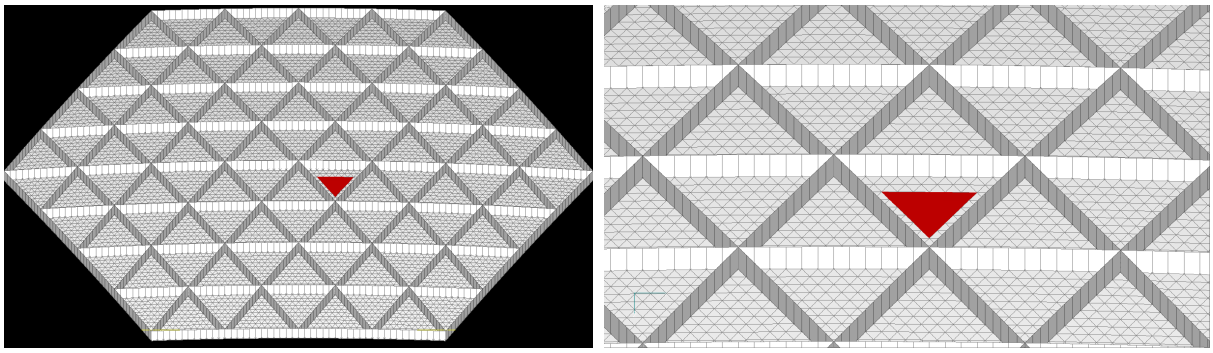

(a) (b)

Figure 11. (a) Sample patch actuator implemented using 2D triangular plate elements and (b) detailed view of the patch actuator.

Figure 12 shows the influence function of the single patch actuator depicted in Figure 11. These results were obtained by using the MOST mirror model and adding a series of 2D CTRIA3 elements to serve as the patch actuator. Following the method used for the cylindrical actuators discussed above, the patch actuator uses thermal analogy to model piezoelectric strains. The resulting influence function is highly localized within the triangular inter-rib region of the facesheet. Future work includes modeling patch actuators throughout the mirror and incorporating their influence functions into the command set (2) to determine the effect on actuator-induced residual error. Such actuators could also help mitigate manufacturing-induced print-through effects as well.[8]

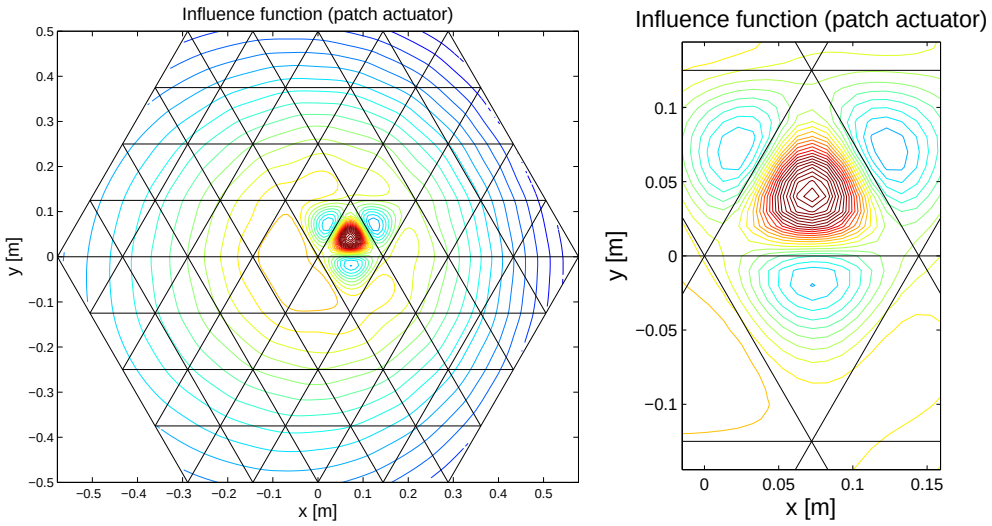

(a) (b)

Figure 12. (a) Influence function of a patch actuator and (b) magnified view of the influence function.

6.2 Optimized rib-stiffened mirror geometry

Key to the work of Budinoff and Michels on SPOT was the identification of a suitable set of basis functions that were used parameterize and then optimize the shape of the mirror substrate. Selecting a set of basis functions is therefore an essential first step in performing geometric optimization. The results presented above point to sinusoidal along-rib shaping as a possible geometric variation to use when optimizing the shape of rib-stiffened active mirrors. Another possibility would be to add smooth blending at the rib-facesheet junction. In current rib-stiffened mirrors, the rib joins the facesheet at a right angle. There is therefore little ability to spread the actuator load from the rib into the adjoining facesheet regions. An example of blended geometry is depicted in Figure 13.

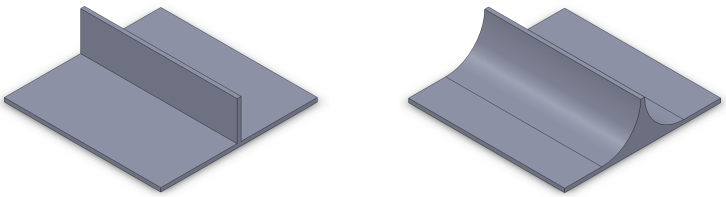

(a) (b)

Figure 13. (a) Standard rib-facesheet intersection (right angle) and (b) blended rib-facesheet intersection. The facesheet is horizontal on the bottom, while the rib is the piece that rises vertically.

Future work would conduct a SPOT-type optimization[5] over mirror shape using the sinusoidal rib basis function identified here and rib-to-facesheet blending. The result would be a design evolution like the one shown in Figure 14. Figure 14(a) represents the current state of rib-stiffened mirror design, in which ribs are constant height and there is no rib-to-facesheet blending. Figure 14(b) shows a mirror incorporating the sinusoidal rib shaping pattern discussed here, which spreads the embedded actuator loads and decreases actuator-induced residual. Figure 14(c) depicts the end-state of an optimization effort: a mirror substrate featuring both rib shaping and rib-to-facesheet blending, both of which reduce actuator-induced residual without increasing areal density. The resulting new design would present manufacturing challenges, given the current methods of casting reaction bonded SiC mirrors. Furthermore, the stiffening effect of the ribs is likely compromised when blending is

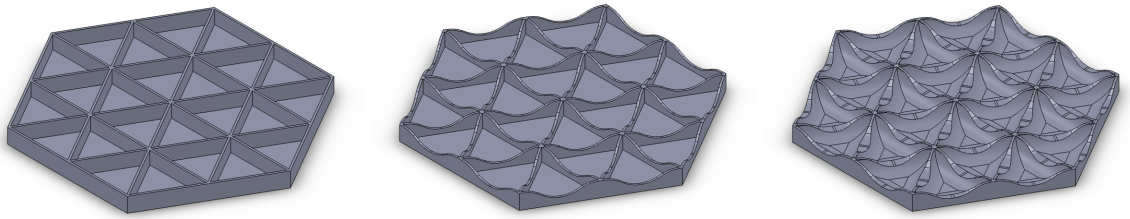

(a) (b) (c)

Figure 14. (a) Standard mirror substrate with constant rib height, (b) mirror substrate with along-rib shaping, and (c) mirror substrate with along-rib shaping and rib-to-facesheet blending. In all cases the facesheet is oriented with its reflecting surface downward.

introduced, therefore a constraint on minimum stiffness would need to be included in the optimization. However, the above results demonstrate that a process of judicious geometric variation could yield a new set of lightweight mirrors with reduced actuator-induced residual error.

REFERENCES

[1] Ealey, M. A. and Wellman, J. A., "Highly adaptive integrated meniscus primary mirrors," *Proc. SPIE* **5166**, 165–171 (2004).

[2] Ealey, M. A. and Weaver, G. Q., "Developmental history and trends for reaction bonded silicon carbide mirrors," *Proc. SPIE* **2857**, 66–72 (1996).

[3] Ealey, M. A., "Integrated actuator meniscus mirror without reaction mass," *United States Patent* **0046976** (March 2005).

[4] Gray, T. L., *Minimizing High Spatial Frequency Residual in Active Space Telescope Mirrors*, Master's thesis, Massachusetts Institute of Technology (2008).

[5] Budinoff, J. G. and Michels, G. J., "Design and optimization of the Spherical Primary Optical Telescope (SPOT) primary mirror segment," *Proc. SPIE* **5877** (2005).

[6] Cohan, L. E. and Miller, D. W., "Vibroacoustic analysis and optimization of lightweight, silicon carbide mirrors," *Proc. SPIE* **7436** (2009).

[7] Cohan, L. E., *Integrated Modeling and Design of Lightweight Active Mirrors for Launch Survival and On-Orbit Performance*, PhD thesis, Massachusetts Institute of Technology (2010).

[8] Gray, T. L., Smith, M. W., Cohan, L. E., and Miller, D. W., "Minimizing high spatial frequency residual in active space telescope mirrors," *Proc. SPIE* **7436** (2009).

[9] Nied, H. F. and Rudmann, A. A., "Temperature induced distortions in space telescope mirrors," *Proc. AIAA Aerospace Sciences* (January 1993).

[10] Shepherd, M. J., Cobb, R. G., Palazotto, A. N., and Baker, W. P., "Modal transformation method for deformable membrane mirrors," *Journal of Guidance, Control, and Dynamics* **32**(1), 276–289 (2009).

[11] Jordan, E. and Miller, D. W., "Primary mirror shape control for athermalization using embedded sensors," *Proc. SPIE* **6687** (2007).

[12] Reed, T., Kendrick, S. E., Brown, R. J., Hadaway, J. B., and Byrd, D., "Final results of the Subscale Beryllium Mirror Demonstrator (SMBD) program," *Proc. SPIE* **4451**, 5–14 (2001).

[13] Chaney, D. M., Brown, R. J., Kendrick, S. E., Reardon, P. J., and Hadaway, J. B., "Results of the beryllium AMSD mirror cryogenic optical testing," *Proc. SPIE* **5487**, 833–841 (2004).

[14] Stahl, H. P., "JWST mirror technology development results," *Proc. SPIE* **6671** (2007).

[15] Stahl, H. P., "JWST lightweight mirror TRL-6 results," *Proc. IEEE Aerospace Conference* , 1–12 (2007).
[16] Park, K.-S., Lee, J. H., and Youn, S.-K., "Lightweight mirror design method using topology optimization," *Opt. Eng.* **44** (May 2005).
[17] Ĉoté, F., Masson, P., Mrad, N., and Cotoni, V., "Dynamic and static modelling of piezoelectric composite structures using a thermal analogy with MSC/NASTRAN," *Composite Structures* **65**, 471–484 (2004).
[18] Dürr, J. K., Honke, R., von Alberti, M., and Sippel, R., "Development and manufacture of an adaptive lightweight mirror for space application," *Smart Materials and Structures* **12**, 1005–1016 (2003).